White matter microstructure underlying default mode network connectivity in the human brain

Stefan J. Teipel, Arun L.W. Bokde, Thomas Meindl, Edson Amaro Jr., Jasmin Soldner, Maximilian F. Reiser, Sabine C. Herpertz, Hans-Jürgen Möller, Harald Hampel

PII: S1053-8119(09)01138-0
DOI: doi:10.1016/j.neuroimage.2009.10.067
Reference: YNIMG 6688

To appear in: *NeuroImage*

Received date: 16 April 2009
Revised date: 16 September 2009
Accepted date: 22 October 2009

Please cite this article as: Teipel, Stefan J., Bokde, Arun L.W., Meindl, Thomas, Amaro Jr., Edson, Soldner, Jasmin, Reiser, Maximilian F., Herpertz, Sabine C., Möller, Hans-Jürgen, Hampel, Harald, White matter microstructure underlying default mode network connectivity in the human brain, *NeuroImage* (2009), doi:10.1016/j.neuroimage.2009.10.067

White matter microstructure underlying default mode network connectivity in the human brain

Stefan J. Teipel [1,2,3], Arun L.W. Bokde[4], Thomas Meindl[5], Edson Amaro Jr.[6], Jasmin Soldner[3], Maximilian F. Reiser[5], Sabine C. Herpertz[1], Hans-Jürgen Möller[3], and Harald Hampel[3,4]

[1]Department of Psychiatry, University Rostock, Rostock, Germany

[2]Deutsches Zentrum für Neurodegenerative Erkrankungen (DZNE), Germany

[3]Department of Psychiatry, Ludwig-Maximilian University, Munich, Germany

[4]Discipline of Psychiatry, School of Medicine and Trinity College Institute of Neuroscience (TCIN), Laboratory of Neuroimaging & Biomarker Research, Trinity College Dublin, The Adelaide and Meath Hospital incorporating the National Children's Hospital (AMiNCH), Dublin, Ireland

[5]Department of Clinical Radiology, University Hospitals – Grosshadern, Ludwig-Maximilian University, Munich, Germany

[6]Department of Radiology, University of Sao Paulo Medical School, Sao Paulo, Brazil

Running Title: White matter microstructure of the default mode network

Manuscript requirements:

Title:	91
Abstract:	237
Text:	5934
References:	55
Tables:	3
Figures	5

Key words: Default mode, resting state fMRI, DTI, functional connectivity, structural connectivity, brain function

Corresponding Author:

Stefan J. Teipel, M.D.
Department of Psychiatry and Psychotherapy,
University Rostock,
Gehlsheimer Str. 20,
18147 Rostock, Germany
Tel.: 01149-381-494-9610
Fax: 01149-381-494-9682
E-mail: stefan.teipel@med.uni-rostock.de

Abstract

Resting state functional magnetic resonance imaging (fMRI) reveals a distinct network of correlated brain function representing a default mode state of the human brain. The underlying structural basis of this functional connectivity pattern is still widely unexplored. We combined fractional anisotropy measures of fiber tract integrity derived from diffusion tensor imaging (DTI) and resting state fMRI data obtained at 3 Tesla from 20 healthy elderly subjects (56 to 83 years of age) to determine white matter microstructure underlying default mode connectivity. We hypothesized that the functional connectivity between the posterior cingulate and hippocampus from resting state fMRI data would be associated with the white matter microstructure in the cingulate bundle and fiber tracts connecting posterior cingulate gyrus with lateral temporal lobes, medial temporal lobes and precuneus. This was demonstrated at the $p < 0.001$ level using a voxel-based multivariate analysis of covariance (MANCOVA) approach. In addition, we used a data driven technique of joint independent component analysis (ICA) that uncovers spatial pattern that are linked across modalities. It revealed a pattern of white matter tracts including cingulate bundle and associated fiber tracts resembling the findings from the hypothesis-driven analysis and was linked to the pattern of default mode network (DMN) connectivity in the resting state fMRI data. Our findings support the notion that the functional connectivity between the posterior cingulate and hippocampus and the functional connectivity across the entire DMN is based on distinct pattern of anatomical connectivity within the cerebral white matter.

Introduction:

Low frequency fluctuations of the BOLD signal in resting state functional magnetic resonance imaging (fMRI) exhibit a complex spatial structure (Cordes et al., 2001) that is believed to correspond to distinct networks which jointly characterize the baseline activity of the human brain (Fox et al., 2005; Hampson et al., 2002). A characteristic set of brain regions, including posterior and anterior cingulate cortex and medial temporal lobes (Greicius et al., 2003b; Raichle et al., 2001), is deactivated during a broad range of cognitive tasks and is believed to support a default mode activity of the human brain. The underling sources of the BOLD signal correlations are still a matter of debate (Chang et al., 2009; Murphy et al., 2009). The detection of a structural basis of the default mode network (DMN) would support a neuronal origin of this connectivity.

Cortical functional connectivity relies on direct and indirect fiber tract connectivity across the cerebral white matter. Fractional anisotropy (FA) derived from diffusion tensor imaging (DTI) provides access to fiber tract integrity in vivo (Stahl et al., 2007). A previous study found significant correlations between connectivity of resting state signal within the grey matter and connectivity of fiber tracts within the white matter (Skudlarski et al., 2008), but could not distinguish between effects from different resting state networks. Two other studies showed that key regions of the DMN were directly connected by fiber tracts reconstructed from DTI (Greicius et al., 2008; van den Heuvel et al., 2008). These studies, however, were restricted to only few regions.

Here, we combined resting state fMRI and DTI data in healthy elderly subjects to determine the underlying white matter microstructure of DMN connectivity. Extensive evidence from animal and human studies shows a close anatomical link between posterior cingulate and hippocampus (Insausti and Munoz, 2001; Lavenex et al., 2002; McIntosh et al., 1996; Suzuki and Amaral, 1994), suggesting that they may be at the core of DMN connectivity. Based on this idea, we hypothesized that the correlation of the resting state

signal between the posterior cingulate and hippocampus would be associated with the FA values of the white matter network connecting the regions of the DMN. The hypothesis was tested using multivariate analysis of variance approach (Teipel et al., 2007). We used previously reported coordinates to derive the time activity curves of posterior cingulate and hippocampus without biasing the results in favor of the subjects under study. In addition, using a purely data driven approach we applied joint independent component analysis (ICA) to determine the common sources of the joint distribution of the fMRI and DTI data without a-priori assumptions on connected brain regions or fiber tracts (Calhoun et al., 2008; Xu et al., 2008). ICA allows accurate separation of the hidden sources from complex signals that arise from the linear mixture of statistically independent signal sources (Hyvarinen and Oja, 2000). We hypothesized that a distinct pattern of white matter fiber tract connectivity, including the cingulate bundle, underlies the functional connectivity within the DMN in the human brain.

Materials and Methods

Subjects

We examined 20 healthy elderly right-handed subjects (mean age: 67.0 (SD 7.3) years, ranging from 56 to 83 years, 9 women). Subjects were recruited among spouses of patients with dementia attending the Memory Clinic at the University Munich, who had no subjective memory complaints and scored within one standard deviation of the age- and education adjusted means of the Mini-Mental-Status Examination (MMSE) (Folstein et al., 1975), CERAD cognitive battery (Berres et al., 2000), Clock-drawing-test (Shulman et al., 1986) and the trail-making test (Chen et al., 2000). The mean MMSE score was 29, SD 0.65, ranging from 28 to 30. Subjects had on average 13.2 (SD 3.7) years of education.

The clinical assessment included detailed medical history, clinical, psychiatric, neurological and neuropsychological examinations, and laboratory tests (complete blood count, electrolytes, glucose, blood urea nitrogen, creatinine, liver-associated enzymes, cholesterol, HDL, triglycerides, serum B12, folate, thyroid function tests, coagulation, serum iron). Additionally, ApoE4 genotyping was performed.

Selection of subjects included a semiquantitative rating of T2-weighted MRI scans (Scheltens et al., 1993). To exclude subjects with significant subcortical cerebrovascular lesions, only subjects were included which had no subcortical white matter hyperintensities exceeding 10 mm in diameter or 3 in number.

All subjects were only examined if they gave their written informed consent. The study was approved by the institutional review board of the Medical Faculty of the University of Munich.

fMRI and DTI acquisition

MRI acquisitions of the brain were conducted with a 3.0 Tesla scanner with parallel imaging capabilities (Magnetom TRIO, Siemens, Erlangen, Germany), maximum gradient strength: 45 mT/m, maximum slew rate: 200T/m/s, 12 element head coil.

Subjects were scanned in a single session without changing their position in the scanner. The following sequences were used: for anatomical reference, a sagittal high-resolution 3-dimensional gradient-echo sequence was performed (magnetization prepared rapid gradient echo MPRAGE, field-of-view 250mm, spatial resolution 0.8 x 0.8 x 0.8 mm^3, repetition time 14 ms, echo time 7.61 ms, flip angle 20^0, number of slices 160). To identify white matter lesions a 2-dimensional T2-weighted sequence was performed (fluid attenuation inversion recovery FLAIR, field-of-view 230 mm, repetition time 9000 ms, echo time 117 ms, voxel size 0.9 x 0.9 x 5.0 mm^3, flip angle 180^0, number of slices 28, acceleration factor 2). Diffusion-weighted imaging was performed with an echo-planar-imaging sequence (field-of-view 256mm, repetition time 9300ms, echo time 102ms, voxel size 2.0 x 2.0 x 2.0mm^3, 4 repeated acquisitions, b-value 1 = 0, b-value 2 = 1000, 12 directions, noise level 10, slice thickness 2.0mm, 64 slices, no overlap). Parallel imaging was performed with a generalized auto-calibrating partially parallel acquisition (GRAPPA, (Griswold et al., 2002)) reconstruction algorithm and an acceleration factor of 2.

The functional imaging sequence was an interleaved T2* weighted echoplanar (EPI) sequence with 28 axial slices (4 mm slice thickness and slice gap = 0.4 mm, repetition time (TR) = 3.0 s, echo time (TE) = 30 ms, flip angle = 90º, field of view = 192 mm. Matrix = 64 x 64) and 120 volumes acquired per subject. The subjects had been instructed to lie quietly with closed eyes and to think about nothing particularly.

DTI data processing

DTI data were preprocessed using the DTI toolbox of the FSL software (http://www.fmrib.ox.ac.uk/fsl/ written mainly by members of the Analysis Group, FMRIB,

Oxford, UK. Version 3.2). After correcting for susceptibility artifacts (Mangin et al., 2002), from the 12 gradient directions and the unweighted scan we estimated the 3x3 diffusion-tensor to extract eigenvalues and eigenvectors to determine fractional anisotropy maps (Teipel et al., 2007). Additionally, mean diffusivity maps (MD) were obtained.

The spatial normalization of FA and MD maps was implemented within Matlab 7.6 (MathWorks, Natwick, Mass.) through Statistical Parametric Mapping (Friston et al., 1995a; Friston et al., 1995b) (SPM 2, Wellcome Department of Imaging Neuroscience, London; available at http://www.fil.ion.ucl.ac.uk/spm), as described in a previous study (Teipel et al., 2007).

In brief, we used low-dimensional normalization with a set of nonlinear basis functions (Ashburner and Friston, 2000; Ashburner et al., 1997) and high-dimensional normalization with symmetric priors (Ashburner et al., 1999) to normalize the anatomical MPRAGE scans into standard space. The low- and high-dimensional normalization parameters were sequentially applied to FA and MD maps that had been spatially coregistered using affine transformation to the anatomical MPRAGE scans in native space. This procedure resulted in FA and MD maps projected into standard space. The anatomical MPRAGE scans in standard space were segmented into CSF, grey matter, and white matter compartments using the SPM2 prior probability maps (Ashburner and Friston, 1997). We expected that the effects of fiber tracts related to DMN connectivity would predominantly be located in the cerebral white matter. Therefore, the data were masked for voxel outside the white matter to consider only effects in the white matter using the binarized anatomical white matter maps.

BOLD sensitive MRI data processing

Data were processed using FSL (FMRIB Software Library – http://www.fmrib.ox.ac.uk/fsl). The initial step was to delete the first 3 volumes of each scan to remove the initial T1 magnetic transients in the data. The remaining data were corrected

for motion effects (6-parameter rigid body), where the reference volume was in the center of the run.

The EPI scans were then registered to the anatomical scan of the same subject in standard space. The anatomical scan was transformed into MNI standard space using affine linear transformation. Both transformations were combined to transform the EPI scans into MNI standard space. The data were band-pass filtered (between 0.01 and 0.15 Hz) and smoothed (Gaussian filter at full width at half maximum = 5 x 5 x 5 mm^3).

Regions of interest

We defined regions of interest (ROI) to derive the time activity curve from selected brain regions. According to previous studies on the functional connectivity within the default mode network, we selected the left and right posterior cingulate gyrus. We extracted the time activity curve using a sphere ROI with radius 6 mm centered around the peak coordinate for the bilateral posterior cingulate gyrus of 2/-51/27 (x/y/z) according to the study by Greicius et al. (2003) (Greicius et al., 2003b). For bilateral hippocampus we used an ROI centered around Talairach-Tournoux coordinates (-)31/-12/-16 (x/y/z) covering the anterior aspect of the hippocampus ROIO used by a previous study (Greicius et al., 2003a). To include only grey matter areas into the ROIs, we masked the sphere ROIs by the grey matter map derived from the respective anatomical MRI scan in the MNI space using automatic segmentation based on a hidden Markov random field model and expectation maximization (Zhang et al., 2001).

Statistical analysis

Default mode network

We used two approaches to analyze the resting state fMRI data that have already been used in earlier studies: voxel-based univariate regression (effective connectivity type of approach) and independent component analysis.

For the univariate approach, we used the time course of the signal within the posterior cingulate gyrus (averaged across both hemispheres) as independent predictor in a voxel-based regression controlling for signal within brain tissue as covariate. In the first level analysis, the regression was performed within subject with a cluster level threshold of $z > 2.3$, $p < 0.05$, corrected for multiple comparisons at the cluster level (Worsley et al., 2002). In the second level analysis, we determined a mixed effects model where effects were thresholded at $z > 2.3$, $p < 0.05$, corrected for multiple comparisons on the cluster level (Beckmann et al., 2003).

To increase the sensitivity of the analysis for detection of medial temporal lobe effects, we determined a second model using a multivariate approach based on ICA. The preprocessed intensity normalized and smoothed (isotropic 5 mm Gaussian kernel) fMRI images were concatenated across subjects to form a single 4D image. The analysis was done using FSL melodic ICA software (www.fmrib.ox.ac.uk/fsl/ melodic/html) (Beckmann and Smith, 2004). ICA determines statistically independent non-Gaussian spatial components from the time-activity signal. Previous studies have used ICA to identify low-frequency neuronal networks during resting state fMRI (Beckmann et al., 2005; Greicius et al., 2004). The algorithm converged on 8 components. From those components the single component best representing the DMN was selected based on visual inspection. Based on a Gaussian/Gamma mixture model using a restricted expectation maximation algorithm we assigned significance to single voxels within the independent component maps (Beckmann et al., 2005). To control the number of false positives, by thresholding the maps at $p > 0.90$ we identified those voxels where the probability to belong to the non-Gaussian active class of voxels was nine-times as high as the probability to belong to the Gaussian random noise class of voxels (Beckmann and Smith, 2004).

Interaction of DTI with fMRI data

To determine the interaction of resting state fMRI and DTI data, we employed two approaches. First, a multivariate analysis of variance (MANOVA) based on principal component analysis where the effects are driven by the functional connectivity between hippocampus and posterior cingulate. Second, an extension of a data driven ICA, where ICA is applied to two different imaging modalities in a single analysis (Calhoun et al., 2008; Xu et al., 2008).

Effects of functional connectivity on FA and MD maps

Within each single subject, the correlations between the time series derived from the posterior cingulate gyrus and hippocampus for the right and left hemisphere were used as measures of functional connectivity between these both core regions of the DMN. We determined the effect of the functional connectivity between both regions on FA and MD maps using multivariate network analysis based on principal component analysis, a method originally developed for activation PET studies by Friston et al. (Friston et al., 1996), adapted to resting state PET data by Zuendorf et al. (Zuendorf et al., 2003), and further extended to MRI and DTI data (Teipel et al., 2007a; Teipel et al., 2007b). This approach is based on the notion that the brain is organized in highly correlated networks where the use of a multivariate analysis captures the common covariance between structurally or functionally connected brain areas. The first step in the analysis is a principal component analysis to reduce the dimensionality of the data. In the second step, the principal components serve as dependent variables to determine the regression of the posterior cingulate hippocampus connectivity on FA and MD values. When the MANOVA yields a significant overall effect, then in the third step the PCA solution space is rotated according to the regression weight of the effect of interest (here: posterior cingulate hippocampus connectivity), to identify the spatial component representing the effect of interest. This component is termed the canonical image or canonical vector. It

represents the spatial distribution of the effect of interest at the significance level determined in the MANOVA.

Prior to principal component analysis, voxels from outside the white matter were removed from the spatially normalized FA and MD maps by means of a mask derived from the white matter maps of the anatomical MPRAGE scans. The masked FA maps were smoothed with a 12-mm FWHM Gaussian kernel. Images were scaled to the same mean value and standard deviation using a voxel-wise z-transformation.

The multivariate approach that was employed in this study has been adapted for DTI data based on the paper by (Friston et al., 1996) in an earlier study (Teipel et al., 2007). We followed three subsequent steps that will only briefly be described in the following section. For further details we refer to (Teipel et al., 2007) and (Friston et al., 1996).

First, the high-dimensionally normalized FA and MD maps were subjected to principal component analysis.

Secondly, we determined the significance of the hypothesized effect of the functional connectivity between posterior cingulate gyrus and hippocampus on FA and MD values using multivariate analysis of covariance (MANCOVA). We employed a linear model with functional connectivity as independent predictor

Thirdly, we characterized the spatial distribution of the effect using canonical variate analysis in terms of the canonical vector that best captured the effect of functional connectivity. To this end, we defined canonical images in the observation space such that the variance ratio between the effect of interest and the total error sum of squares was maximized. Each canonical image has an associated canonical value that serves to estimate whether a particular canonical image is important. The canonical value can be compared to an F distribution with nominator degrees of freedom equal to the rank of the matrix of the effect of interest and denominator degrees of freedom equal to the number of scans minus the rank of

the design matrix (= degrees of freedom of the error term). We considered a canonical image important if its canonical value exceeded the critical F threshold for $p < 0.05$.

Calculations were carried out using an algorithm written in MATLAB v. 7.6 (Mathworks, Newton, MA).

Joint independent component analysis of resting state fMRI and DTI data

To determine the association between DMN connectivity and white matter microstructure without a priori selection of correlated regions, we applied the newly published approach of joint ICA (Calhoun et al., 2008; Xu et al., 2008). ICA assumes that a given data distribution results from the linear mixing of a set of unknown sources of signal that can be estimated when the hidden signal sources are statistically independent and arise from some non-gaussian distribution. Joint ICA determines the hidden sources of a joint data distribution from different imaging modalities to uncover spatial pattern that are linked across modalities. Analysis was performed using the joint ICA toolbox (JICAT v1.2a) implemented in Matlab 7.0 (available at http://icatb.sourceforge.net). Contrast images of the fMRI data for each subject were determined using posterior cingulate gyrus activity as regressor as described above using FSL. Spatially normalized and white matter masked FA maps were used for the DTI data. FMRI and DTI data were sampled to have a common voxel size (2.0 mm^3) and normalized to have the same average sum-of-squares (computed across all subjects and all voxels for each modality). The normalization step accounted for different ranges in signal intensities between fMRI and DTI data by preserving the scaling within modality, but normalizing units between modalities. FMRI and DTI data were combined in one data matrix that was subjected to ICA. Based on the previous ICA analysis of the fMRI data and the PCA of the DTI data, the algorithm was instructed to search for 8 components. Repetition, however, with a larger or smaller number of components (6 to 15) resulted in almost identical findings in respect to the DMN component. The independent component of the fMRI data

most closely resembling the DMN was selected and compared to the joint component from the DTI data.

Results

Default mode network

The regression of the posterior cingulate time series using the mixed-effects second level framework revealed the characteristic DMN pattern compromising posterior cingulate gyrus, precuneus, superior parietal lobules, anterior cingulate, medial prefrontal cortex, dorsolateral prefrontal cortex, infero-lateral temporal lobe, and thalamus (Figure 1, Table 1). Medial temporal lobe areas were not included in this network. Using ICA, we found a more extended network including the previous areas but additionally compromising activated areas in the fusiform gyrus extending into parahippocampal gyrus and hippocampus, as well as middle occipital and lingual gyrus (Figure 2).

- Figures 1 and 2 and Table 1 near here -

Effect of correlations between posterior cingulate and hippocampus resting state activity on regional FA

Applying principle component analysis reduced the dimensionality of the FA data to 8 eigenimages with eigenvalues greater than 1. Separate MANCOVAs revealed significant effects with Wilks lambda after transformation equal to 21.44, 8 df, $p < 0.01$ for the correlations between left posterior cingulate and hippocampus and Wilks lambda after transformation equal to 21.09, 8 df, $p < 0.01$ for the correlations between right posterior cingulate and hippocampus. The canonical values associated with the second canonical image were 92.75 for the left correlations and 63.17 for the right correlations, both being larger than the threshold $F_{18}^{1} = 8.29$ for $p < 0.01$.

Higher correlations between posterior cingulate and hippocampus in the left and the right hemisphere were significantly associated with higher FA in bilateral precuneus, extending to posterior cingulate, lingual, fusiform, and parahippocampal gyrus, hippocampus, as well as lateral and basal temporal lobe white matter. Particularly, the canonical analysis detected large parts of the cingulate bundle directly connecting posterior cingulate gyrus with

anterior cingulate gyrus, hippocampus and precuneus (figure 3b). Additionally, posterior corpus callosum, insula, fornix, thalamus, inferior parietal lobule and cerebellum white matter were involved (Tables 2 and 3, Figure 3).

- Figure 3 and Tables 2 and 3 near here –

The age effect on the interaction between DTI and fMRI data was not significant. Separate MANCOVAs revealed significant effects with Wilks lambda after transformation equal to 24.67, 8 df, $p < 0.01$ for the correlations between left posterior cingulate and hippocampus and Wilks lambda after transformation equal to 20.62, 8 df, $p < 0.01$ for the correlations between right posterior cingulate and hippocampus, after controlling for age. The canonical values associated with the second canonical image were 94.4 for the left correlations and for the right correlations 66.10 after controlling for age, both being larger than the threshold $F_{18}^{1} = 8.29$ for $p < 0.01$. There was a very close overlap between the regional distribution of the spatial components before and after including age as covariate reflecting the effect of post cingulate to hippocampus connectivity on the FA maps

Effect of correlations between posterior cingulate and hippocampus resting state activity on regional MD

Applying principle component analysis reduced the dimensionality of the MD data to 6 eigenimages with eigenvalues greater than 1. Separate MANCOVAs revealed significant effects with Wilks lambda after transformation equal to 24.08, 6 df, $p < 0.001$ for the correlations between left posterior cingulate and hippocampus, and Wilks lambda after transformation equal to 13.41, 6 df, $p < 0.1$ for the correlations between right posterior cingulate and hippocampus. The canonical value associated with the first canonical image was 71.60 for the left correlation, being larger than the threshold = 8.29 for $p < 0.01$, the effect for the right post cingulated hippocampus correlation was not significant.

Higher correlations between posterior cingulate and hippocampus in the left hemisphere were significantly associated with lower MD in white matter areas connecting posterior cingulated and hippocampus, and lateral temporal lobes. Additionally, there were areas in the anterior cingulated gyrus and the lingual gyrus as well as in the cerebellum. There were no white matter areas involved connecting posterior cingulated with superior parietal lobules.

- Figure 4 near here –

Joint independent component analysis

Results from the joint ICA of the fMRI and DTI data are shown in figure 4. One of 8 components for the fMRI data showed the typical features of the DMN including posterior cingulate, precuneus, anterior cingulate and medial prefrontal cortex, lateral temporal cortex, medial temporal lobe, including hippocampus and parahippocampal gyrus, as well as thalamus grey matter. The corresponding source of the DTI data showed cingulate bundle from posterior to anterior cingulate, extending to superior parietal, as well as lateral and medial temporal lobes. Addtionally there was a fiber bundle extending into midbrain and along the superior cerebellar pedunculi.

- Figure 5 near here –

The mixing matrix describing the separation of the joint components of the DMN in the fMRI and DTI data was independent from age ($r = -0.11$, $p = 0.66$).

Discussion

We investigated the regional pattern of white matter microstructure underlying functional connectivity within the resting state DMN. Both a hypothesis-driven approach based on functional connectivity of posterior cingulate and a data driven ICA approach recovered the key regions of the DMN in the resting state fMRI data. When we regressed the functional connectivity between posterior cingulate and hippocampus on the FA maps of white matter microstructure we found distinct subcortical white matter areas matching the distribution of DMN components. Agreeing with and extending this finding, a purely data driven joint ICA across modalities revealed a distinct pattern of white matter tract integrity that was linked to the functional connectivity within the DMN.

Using linear regression, posterior cingulate gyrus BOLD activity was correlated with the activity in posterior cingulate, medial frontal and anterior cingulate gyrus, lateral temporal lobes and precuneus, replicating findings from earlier studies (Damoiseaux et al., 2006; Fransson, 2005; Greicius et al., 2003b; Raichle et al., 2001).

Consistent with this pattern, the ICA approach identified one single spatial component encompassing the key regions of the default mode network and extending into medial temporal lobe areas including hippocampus. Hippocampus is believed to be a key region of the default mode network (Greicius et al., 2004), but has not been recovered at 3 Tesla (Greicius et al., 2003b) using an univariate approach, possibly due to susceptibility artifacts (Krasnow et al., 2003). Our data suggest that an ICA approach is more powerful than univariate analysis to detect the involvement of the hippocampus at 3 Tesla, possibly related to the ability of ICA to separate different biological and non-biological sources of the signal. The DMN component in our study closely resembled the spatial pattern reported in previous studies using multisubject ICA (Esposito et al., 2008; Greicius et al., 2004), but was spatially more extended. The previous studies had combined the independent components from single subject data most resembling the DMN in a random effects analysis on the group level. The a

priori selection of the template used to measure the fit between the component and the DMN will bias the selection of the component in each subject. This type of bias does not occur in the fixed effects type of analysis in our study where the volumes were concatenated across time for all subjects. To protect the analysis against false positives we chose a very conservative threshold for the posterior probability of a voxel not representing random correlation.

Comparing the wide-spread effects in our elderly subjects including medial temporal lobe areas with effects reported on younger subjects (Damoiseaux et al., 2006; Fransson, 2005; Greicius et al., 2003b; Greicius et al., 2004; Raichle et al., 2001), our data suggest that in cognitively healthy elderly subjects the main components of the DMN are well preserved. In a previous study, DMN connectivity was reduced in elderly compared to younger subjects with age accounting for about 19% of variation in the fit of individual independent components to a predefined DMN template (Esposito et al., 2008). The main components, however, of the DMN had been preserved in the previous study, as well. Additionally, the authors had employed random effect type group ICA where the effect of age depended on the template used to select the independent components representing the DMN in each individual subject (Esposito et al., 2008).

The main objective of our study was to determine the association between functional connectivity within the DMN and anatomical connectivity across the white matter. Using a MANCOVA approach we found that the functional connectivity between posterior cingulate and hippocampus (PCC-Hipp) was correlated with FA along subcortical fiber tracts directly connecting both brain regions. The spatial component reflecting the association of PCC-Hipp functional connectivity with the white matter microstructure included all posterior brain areas that have been associated with the DMN. In addition, consistent with the involvement of medial prefrontal and anterior cingulate cortex in the DMN, we found that the PCC-Hipp functional connectivity was associated with fiber tract integrity along the cingulate white

matter as well as with white matter areas directly connecting posterior cingulate and lateral temporal lobe areas, including middle and inferior temporal gyrus, as well as white matter areas extending from posterior cingulate gyrus to precuneus. Finally, we found associations of PCC-Hipp functional connectivity with white matter areas of the insula, and lingual, middle occipital and fusiform gyrus. All of these brain regions were involved in the independent component most closely representing the DMN in our subjects. Thus, although we used the functional connectivity of only two subregions of the DMN as regressor we uncovered large parts of the entire cingulate bundle and associated white matter tracts (Schmahmann et al., 2007). This finding suggests that the DMN network changes as a single unit so that the functional connectivity of its subregions serves as a proxy for the functional connectivity within the entire network. Previous studies have suggested that the human brain is intrinsically organized into networks (Fox et al., 2005; Fox et al., 2009) which has been also found in monkeys (Vincent et al., 2007). The detection of a distinct pattern of fiber tract connectivity suggests that DMN connectivity may be a reflection of a fundamental property of the organization of the human brain and not only of vascular components, as previously suggested (Birn et al., 2006).

Our data agree with and extend previous reports on fiber tracts that were associated with DMN connectivity in resting state fMRI data (Greicius et al., 2008; van den Heuvel et al., 2008). Greicius et al. (Greicius et al., 2008) performed fiber tracking between three seed points that represented peak coordinates of the resting state network. They found direct tracts from posterior cingulate gyrus to hippocampus and medial prefrontal cortex, but no tracts between hippocampus and medial prefrontal cortex. Similarly, van den Heuvel et al. (van den Heuvel et al., 2008) used an ROI-approach, where the FA values were averaged across a fiber tract detected between few peak regions of the DMN. These studies supported anatomical evidence from primate studies that key regions of the DMN have direct anatomical connections. Our study differs from these earlier studies in three important aspects. First, we

defined the coordinates of the regions of interest from an independent sample reported in the literature (Greicius et al., 2003b) to avoid circular conclusions where the detection of an effect at a specific location drives the selection of this location to detect an effect. Secondly, we used a statistical approach to assess whether the degree of functional connectivity within the DMN correlates with the integrity of white matter microstructure. Thirdly, we considered not only few peak regions but regressed the PCC-Hipp functional connectivity on the entire cerebral white matter microstructure.

The spatial distribution of decreased MD with higher connectivity was similar to the spatial distribution of increased FA with higher connectivity, but there were also differences. Similar to the FA maps, there were fiber tract areas connecting hippocampus and posterior cingulate in both hemispheres, as well as fiber tracts connecting posterior cingulate with precuneus and anterior cingulate. With MD, however, effects were more pronounced in the anterior cingulate compared to FA, whereas with FA, there were stronger effects for fiber tracts projecting into superior parietal lobe areas. Both microstructural features, however, captured fiber tracts connecting essential parts of the default mode network. FA represents the anisotropy within the fiber system related to the directionality of fiber tracts, whereas MD represents the overall diffusivity representing loss of fiber tract directionality. The less specific regional pattern of MD compared to FA, however, suggests that FA is the more specific microstructural marker to detect fiber tract integrity underlying neuronal network connectivity.

To confirm our findings using a purely data driven approach, we applied the technique of joint ICA (Calhoun et al., 2006). This approach decomposes two features (here fMRI and DTI), both collected on every individual, into a joint set of components that represent maximally spatially independent components. We found a single pattern of grey matter regions representing the DMN as well as an associated single pattern of white matter microstructure that connected all key regions of the DMN including cingulate bundle with

connections into medial prefrontal lobes and anterior cingulate gyrus as well as direct connections between posterior cingulate gyrus and precuneus, lateral and medial temporal lobes. Comparing the white matter tracts recovered using MANCOVA with the tracts recovered by joint ICA, both approaches converged in the posterior brain areas. The joint ICA approach, however, showed additional white matter areas projecting onto the superior longitudinal fasciculus, connecting medial and lateral prefrontal lobe regions with lateral temporal lobes, onto the arcuate bundle, connecting lateral prefrontal with superior temporal lobe areas (Schmahmann et al., 2007), and onto corpus callosum splenium, connecting association areas of posterior temporal and parietal lobes (De Lacoste et al., 1985). Additionally, the ICA approach showed white matter areas in the internal capsule extending to thalamus, midbrain and cerebellum. This finding agrees with the involvement of the thalamus and the cerebellum in DMN connectivity (Greicius et al., 2007; Marchand et al., 2007).

The wider extension of the findings in the ICA approach is not unexpected, as the MANCOVA was driven by posterior cingulate and hippocampus connectivity that may be stronger associated with anterior cingulate and parietal lobe brain areas than with prefrontal lobe areas (Wakana et al., 2004). In contrast, the joint ICA approach was driven by the entire DMN and therefore was able to detect besides others the whiter matter connections into the prefrontal lobes. To our knowledge this is the first time that joint ICA has been applied to combined resting state fMRI and DTI data. The convergent results with the MANCOVA approach support the use of joint ICA.

There are potential limitations to be discussed with our study. First, aging has been associated with both, reduced connectivity within the DMN (Esposito et al., 2008) and reduced subcortical fractional anisotropy (Zhang et al., 2008). After controlling for age, however, our findings remained essentially unchanged, supporting the specificity of the

effects for underlying regional networks and not for an effect of age on both functional connectivity and fiber tract integrity.

Second, the analysis of the FA maps relies on the normalization of the data into standard space based on the anatomical scans. A critical step in this procedure is the affine co-registration between the FA maps and the anatomical scans in native space. As DTI sequences are prone to susceptibility related distortions, in our experience the fit between a DTI sequence and anatomical scans is most difficult for frontal lobe areas, specifically fronto-basal areas. By employing parallel imaging at 3 Tesla, we could considerably reduce distortion related artefacts in our acquisitions as described in a previous paper (Stahl et al., 2007). The fit of the FA maps with the anatomical scans was excellent by visual inspection, even the frontal lobes showed a very close fit (figures S1 and S2, supplementary material). However, an effect on residual distortions can not be excluded within the framework of the method.

Third, the selection for the smoothing kernel of the FA maps remains arbitrary, but could affect the findings of a study. To assess this effect in our study, we repeated the analysis after smoothing with an 8 mm, instead of a 12 mm FWHM Gaussian kernel. The findings remained essentially unchanged, the spatial distribution of the effects of the analysis after 8 mm smoothing were almost entirely contained within the spatial distribution of the effects after 12 mm smoothing (figure S3, supplementary material).

Finally, the selection of the masking procedure of the FA and MD maps may have had an influence on the findings. To assess this effect, we determined the effect of HIPP-PC connectivity on the segmented white matter maps that were used to mask the FA and MD maps for tissue outside the white matter. We subjected these maps to an analogous PCA as the FA and MD maps after smoothing with a 12 mm FWHM Gaussian kernel. The white matter maps were not binarized in this analysis, but the intensity at each voxel represented the probability of this voxel to belong to the cerebral white matter. There was a significant effect of bilateral PC-HIPP connectivity on white matter ($p < 0.01$), however, there was almost no

overlap between the effect on the white matter and the effect on FA or MD (figures S4 and S5, supplementary material). The effects on white matter were much more widespread and less specifically distributed throughout the white matter. These findings suggest that the segmentation does not account for the effects of PC-HIPP connectivity on FA maps, and that FA is a more specific measure of white matter microstructural integrity than segmented white matter density.

In summary, the pattern of DMN functional connectivity was significantly associated with a consistent pattern of white matter microstructure in cingulate bundle and associated fiber tracts both in multivariate statistical analysis and purely data driven detection of hidden signal sources. Therefore, extending earlier evidence from ROI-based analyses our data suggest that DMN connectivity is based on a distinct pattern of fiber tract connectivity in healthy elderly subjects. In addition, we introduced a new approach of analyzing the functional and structural networks underlying the DMN. It will be the goal of subsequent studies to determine the association between functional and structural connectivity within the DMN in neurodegenerative disorders known to impair intracortical connectivity.

Acknowledgment

Part of this work was supported by grants of the Medical Faculty of the Ludwig-Maximilian University (Munich, Germany) to S.J.T., of the Hirnliga e. V. (Nürmbrecht, Germany) to S.J.T., an investigator initiated unrestricted research grant from Janssen-CILAG (Neuss, Germany) to H.H. and S.J.T., and a grant from the Bundesministerium für Bildung und Forschung (BMBF 01 GI 0102) awarded to the dementia network "Kompetenznetz Demenzen". Further funding was obtained through the Science Foundation Ireland (SFI) Stokes Programme (to A.L.W.B.), and through the SFI investigator neuroimaging programme grant 08/IN.1/B1846 (H.H.). There are no conflicts of interest associated with the work presented in this article.

References:

Ashburner, J., Andersson, J.L., Friston, K.J., 1999. High-dimensional image registration using symmetric priors. Neuroimage 9, 619-628.

Ashburner, J., Friston, K., 1997. Multimodal image coregistration and partitioning--a unified framework. Neuroimage 6, 209-217.

Ashburner, J., Friston, K.J., 2000. Voxel-based morphometry--the methods. Neuroimage 11, 805-821.

Ashburner, J., Neelin, P., Collins, D.L., Evans, A., Friston, K., 1997. Incorporating prior knowledge into image registration. Neuroimage 6, 344-352.

Beckmann, C.F., DeLuca, M., Devlin, J.T., Smith, S.M., 2005. Investigations into resting-state connectivity using independent component analysis. Philos Trans R Soc Lond B Biol Sci 360, 1001-1013.

Beckmann, C.F., Jenkinson, M., Smith, S.M., 2003. General multilevel linear modeling for group analysis in FMRI. Neuroimage 20, 1052-1063.

Beckmann, C.F., Smith, S.M., 2004. Probabilistic independent component analysis for functional magnetic resonance imaging. IEEE Trans Med Imaging 23, 137-152.

Berres, M., Monsch, A.U., Bernasconi, F., Thalmann, B., Stahelin, H.B., 2000. Normal ranges of neuropsychological tests for the diagnosis of Alzheimer's disease. Stud Health Technol Inform 77, 195-199.

Birn, R.M., Diamond, J.B., Smith, M.A., Bandettini, P.A., 2006. Separating respiratory-variation-related fluctuations from neuronal-activity-related fluctuations in fMRI. Neuroimage 31, 1536-1548.

Calhoun, V.D., Adali, T., Giuliani, N.R., Pekar, J.J., Kiehl, K.A., Pearlson, G.D., 2006. Method for multimodal analysis of independent source differences in schizophrenia: combining gray matter structural and auditory oddball functional data. Hum. Brain Mapp. 27, 47-62.

Calhoun, V.D., Liu, J., Adali, T., 2008. A review of group ICA for fMRI data and ICA for joint inference of imaging, genetic, and ERP data. Neuroimage.

Chang, C., Cunningham, J.P., Glover, G.H., 2009. Influence of heart rate on the BOLD signal: the cardiac response function. Neuroimage 44, 857-869.

Chen, P., Ratcliff, G., Belle, S.H., Cauley, J.A., DeKosky, S.T., Ganguli, M., 2000. Cognitive tests that best discriminate between presymptomatic AD and those who remain nondemented. Neurology 55, 1847-1853.

Cordes, D., Haughton, V.M., Arfanakis, K., Carew, J.D., Turski, P.A., Moritz, C.H., Quigley, M.A., Meyerand, M.E., 2001. Frequencies contributing to functional connectivity in the cerebral cortex in "resting-state" data. AJNR Am J Neuroradiol 22, 1326-1333.

Damoiseaux, J.S., Rombouts, S.A., Barkhof, F., Scheltens, P., Stam, C.J., Smith, S.M., Beckmann, C.F., 2006. Consistent resting-state networks across healthy subjects. Proc Natl Acad Sci U S A 103, 13848-13853.

De Lacoste, M.C., Kirkpatrick, J.B., Ross, E.D., 1985. Topography of the human corpus callosum. J. Neuropath. Exper. Neurol. 44, 578-591.

Esposito, F., Aragri, A., Pesaresi, I., Cirillo, S., Tedeschi, G., Marciano, E., Goebel, R., Di Salle, F., 2008. Independent component model of the default-mode brain function: combining individual-level and population-level analyses in resting-state fMRI. Magn Reson Imaging 26, 905-913.

Folstein, M.F., Folstein, S.E., McHugh, P.R., 1975. Mini-mental-state: a practical method for grading the cognitive state of patients for the clinician. J. Psychiatr. Res. 12, 189-198.

Fox, M.D., Snyder, A.Z., Vincent, J.L., Corbetta, M., Van Essen, D.C., Raichle, M.E., 2005. The human brain is intrinsically organized into dynamic, anticorrelated functional networks. Proc. Natl. Acad. Sci. USA 102, 9673-9678.

Fox, M.D., Zhang, D., Snyder, A.Z., Raichle, M.E., 2009. The Global Signal and Observed Anticorrelated Resting State Brain Networks. J Neurophysiol.

Fransson, P., 2005. Spontaneous low-frequency BOLD signal fluctuations: an fMRI investigation of the resting-state default mode of brain function hypothesis. Hum Brain Mapp 26, 15-29.

Friston, K., Ashburner, J., Frith, C.D., Poline, J.-B., Heather, J.D., Frackowiak, R.S.J., 1995a. Spatial registration and normalization of image. Hum. Brain Mapp. 2, 165-189.

Friston, K., Holmes, A.P., Worsley, K., Poline, J.-B., C.D., F., Frackowiak, R.S.J., 1995b. Statistical parametric maps in functional imaging: a general linear approach. Hum Brain Mapp 2, 189-210.

Friston, K.J., Poline, J.P., Holmes, A.P., Frith, C., Frackowiak, R.S.J., 1996. A multivariate analysis of PET activation studies. Hum. Brain Map. 4, 140-151.

Greicius, M.D., Flores, B.H., Menon, V., Glover, G.H., Solvason, H.B., Kenna, H., Reiss, A.L., Schatzberg, A.F., 2007. Resting-state functional connectivity in major depression: abnormally increased contributions from subgenual cingulate cortex and thalamus. Biol Psychiatry 62, 429-437.

Greicius, M.D., Krasnow, B., Boyett-Anderson, J.M., Eliez, S., Schatzberg, A.F., Reiss, A.L., Menon, V., 2003a. Regional analysis of hippocampal activation during memory encoding and retrieval: fMRI study. Hippocampus 13, 164-174.

Greicius, M.D., Krasnow, B., Reiss, A.L., Menon, V., 2003b. Functional connectivity in the resting brain: a network analysis of the default mode hypothesis. Proc. Natl. Acad. Sci. USA 100, 253-258.

Greicius, M.D., Srivastava, G., Reiss, A.L., Menon, V., 2004. Default-mode network activity distinguishes Alzheimer's disease from healthy aging: evidence from functional MRI. Proc Natl Acad Sci U S A 101, 4637-4642.

Greicius, M.D., Supekar, K., Menon, V., Dougherty, R.F., 2008. Resting-State Functional Connectivity Reflects Structural Connectivity in the Default Mode Network. Cereb Cortex.

Griswold, M.A., Jakob, P.M., Heidemann, R.M., Nittka, M., Jellus, V., Wang, J., Kiefer, B., Haase, A., 2002. Generalized autocalibrating partially parallel acquisitions (GRAPPA). Magn. Reson. Med. 47, 1202-1210.

Hampson, M., Peterson, B.S., Skudlarski, P., Gatenby, J.C., Gore, J.C., 2002. Detection of functional connectivity using temporal correlations in MR images. Hum. Brain Mapp. 15, 247-262.

Hyvarinen, A., Oja, E., 2000. Independent component analysis: algorithms and applications. Neuronal Networks 13, 411-430.

Insausti, R., Munoz, M., 2001. Cortical projections of the non-entorhinal hippocampal formation in the cynomolgus monkey (Macaca fascicularis). Eur J Neurosci 14, 435-451.

Krasnow, B., Tamm, L., Greicius, M.D., Yang, T.T., Glover, G.H., Reiss, A.L., Menon, V., 2003. Comparison of fMRI activation at 3 and 1.5 T during perceptual, cognitive, and affective processing. Neuroimage 18, 813-826.

Lavenex, P., Suzuki, W.A., Amaral, D.G., 2002. Perirhinal and parahippocampal cortices of the macaque monkey: projections to the neocortex. J Comp Neurol 447, 394-420.

Mangin, J.F., Poupon, C., Clark, C., Le Bihan, D., Bloch, I., 2002. Distortion correction and robust tensor estimation for MR diffusion imaging. Med Image Anal 6, 191-198.

Marchand, W.R., Lee, J.N., Thatcher, J.W., Thatcher, G.W., Jensen, C., Starr, J., 2007. Motor deactivation in the human cortex and basal ganglia. Neuroimage 38, 538-548.

McIntosh, A.R., Grady, C.L., Haxby, J.V., Ungerleider, L.G., Horwitz, B., 1996. Changes in limbic and prefrontal functional interactions in a working memory task for faces. Cereb Cortex 6, 571-584.

Murphy, K., Birn, R.M., Handwerker, D.A., Jones, T.B., Bandettini, P.A., 2009. The impact of global signal regression on resting state correlations: are anti-correlated networks introduced? Neuroimage 44, 893-905.

Raichle, M.E., MacLeod, A.M., Snyder, A.Z., Powers, W.J., Gusnard, D.A., Shulman, G.L., 2001. A default mode of brain function. Proc Natl Acad Sci U S A 98, 676-682.

Scheltens, P., Barkhof, F., Leys, D., Pruvo, J.P., Nauta, J.J.P., Vermersch, P., Steinling, M., Valk, J., 1993. A semiquantitative rating scale for the assessment of signal hyperintensities on magnetic resonance imaging. J. Neurol. Sci. 114, 7-12.

Schmahmann, J.D., Pandya, D.N., Wang, R., Dai, G., D'Arceuil, H.E., de Crespigny, A.J., Wedeen, V.J., 2007. Association fibre pathways of the brain: parallel observations from diffusion spectrum imaging and autoradiography. Brain 130, 630-653.

Shulman, K.I., Shedletsky, R., Silver, I.L., 1986. The challenge of time: Clock drawing and cognitive function in the elderly. Int. J. Geriatr. Psychiatry 1, 135-140.

Skudlarski, P., Jagannathan, K., Calhoun, V.D., Hampson, M., Skudlarska, B.A., Pearlson, G., 2008. Measuring brain connectivity: Diffusion tensor imaging validates resting state temporal correlations. Neuroimage.

Stahl, R., Dietrich, O., Teipel, S.J., Hampel, H., Reiser, M.F., Schoenberg, S.O., 2007. White matter damage in Alzheimer's disease and in mild cognitive impairment: assessment with diffusion tensor MRI using parallel imaging techniques. Radiology 243, 483-492.

Suzuki, W.A., Amaral, D.G., 1994. Perirhinal and parahippocampal cortices of the macaque monkey: cortical afferents. J Comp Neurol 350, 497-533.

Talairach, J., Tournoux, P., 1988. Co-Planar Stereotaxic Atlas of the Human Brain. Thieme, New York.

Teipel, S.J., Stahl, R., Dietrich, O., Schoenberg, S.O., Perneczky, R., Bokde, A.L., Reiser, M.F., Moller, H.J., Hampel, H., 2007. Multivariate network analysis of fiber tract integrity in Alzheimer's disease. Neuroimage 34, 985-995.

van den Heuvel, M., Mandl, R., Luigjes, J., Hulshoff Pol, H., 2008. Microstructural organization of the cingulum tract and the level of default mode functional connectivity. J Neurosci 28, 10844-10851.

Vincent, J.L., Patel, G.H., Fox, M.D., Snyder, A.Z., Baker, J.T., Van Essen, D.C., Zempel, J.M., Snyder, L.H., Corbetta, M., Raichle, M.E., 2007. Intrinsic functional architecture in the anaesthetized monkey brain. Nature 447, 83-86.

Wakana, S., Jiang, H., Nagae-Poetscher, L.M., van Zijl, P.C., Mori, S., 2004. Fiber tract-based atlas of human white matter anatomy. Radiology 230, 77-87.

Worsley, K.J., Liao, C.H., Aston, J., Petre, V., Duncan, G.H., Morales, F., Evans, A.C., 2002. A general statistical analysis for fMRI data. Neuroimage 15, 1-15.

Xu, L., Pearlson, G., Calhoun, V.D., 2008. Joint source based morphometry identifies linked gray and white matter group differences. Neuroimage.

Zhang, Y., Brady, M., Smith, S., 2001. Segmentation of brain MR images through a hidden Markov random field model and the expectation maximization algorithm. EEE Trans. on Medical Imaging 20, 45-57.

Zhang, Y., Du, A.T., Hayasaka, S., Jahng, G.H., Hlavin, J., Zhan, W., Weiner, M.W., Schuff, N., 2008. Patterns of age-related water diffusion changes in human brain by concordance and discordance analysis. Neurobiol Aging (e-pub ahead of print).

Figures

Figure 1: Resting-state connectivity of the posterior cingulate gyrus (mixed effects analysis)

The map of the resting-state connectivity of the posterior cingulate gyrus is superimposed on the rendered surface projection of the anatomical template brain in standard space. Effects were thresholded at $p < 0.05$, corrected for multiple comparisons on the cluster level

Axial slices go from ventral at Talairach-Tournoux coordinate z = -16 to dorsal at z = 48, sections are 6 mm apart.

L = left

Figure 2: Resting-state connectivity in the DMN (independent component analysis)

The map of the resting-state connectivity from independent component analysis most resembling the DMN pattern is superimposed on the rendered surface projection of the anatomical template brain in standard space. Effects were thresholded at posterior probability of $p > 0.90$.

Figure 2a: Axial slices go from ventral at Talairach-Tournoux coordinate z = -16 to dorsal at z = 48, sections are 6 mm apart.

Figure 2b: The coronal slice goes through Talairach Tournoux-coordinate y = -17, illustrating the involvement of medial temporal lobe areas in the DMN (blue arrows)

Figure 3: Functional connectivity between posterior cingulate and hippocampus and FA

The positive components of the second canonical images with left posterior cingulate-hippocampus connectivity (red) and right posterior cingulate-hippocampus connectivity (blue) regressed on FA, representing higher FA values with higher connectivity. The effects are projected on the rendered axial sections of the T1-weighted template brain (Figure 3a), and paramidsagittal sections (Figure 3b). Axial sections go from ventral at

Talairach-Tournoux coordinate z = -16 to dorsal at z = 48, sections are 6 mm apart. Right of image is right of brain (view from superior). Sagittal sections go from Talairach-Tournoux coordinate x = 4 to x = 27 (right), and x = -4 to x = -27 (left), sections are 3 mm apart.

Red arrows point to the cingulate white matter, green arrows point to fiber tracts connecting posterior cingulate and hippocampus/parahippocampal gyrus.

Figure 4: Functional connectivity between posterior cingulate and hippocampus and MD

The negative components of the first canonical image with left posterior cingulate-hippocampus connectivity (red) regressed on MD, representing higher MD values with lower connectivity. The effects are projected on the rendered axial sections of the T1-weighted template brain. Axial sections go from ventral at Talairach-Tournoux coordinate z = -16 to dorsal at z = 48, sections are 6 mm apart. Right of image is right of brain (view from superior).

Figure 5: Figure 4: Joint ICA of fMRI and DTI data

Component 6 of 8 demonstrated the DMN feature in the fMRI data. The joint source map for the fMRI (top) and the DTI data (bottom) is projected on the sagittal sections of a T1-weighted template brain in standard space, sagittal sections go from Talairach-Tournoux coordinate x = -39 to x = 39, sections are 4 mm apart.

Table 1: Resting state connectivity (mixed effects model)

Region	Side	BA	Maximal z-score primary peak	Primary peak Coordinates (mm)		
				x	y	z
Cingulate gyrus / posterior cingulate / precuneus	L	31/29	8.55	-4.0	-50.0	26.0
Medial frontal gyrus / anterior cingulate	L	10/9/32/8	6.2	-5.0	55.0	13.0
Middle temporal gyrus / superior temporal gyrus	L	39	5.78	-50.0	-61.0	25.0
Superior temporal gyrus / middle temporal gyrus / precuneus	R	22/39	5.53	55.0	-58.0	17.0
Middle temporal gyrus / inferior temporal gyrus	L	21/20	5.31	-63.0	-32.0	-15.0
Globus pallidus / Putamen / Thalamus (VAN, Pulvinar)	L	-	5.12	-15.0	0.0	8.0
Putamen / Thalamus (VAN, VLN)	R	-	3.56	17.0	0.0	12.0

Peak coordinates are indicated by Talairach and Tournoux coordinates, x, y and z (Talairach and Tournoux, 1988): x = the medial to lateral distance relative to midline (positive = right hemisphere); y = the anterior to posterior distance relative to the anterior commissure (positive = anterior); z = superior to inferior distance relative to the anterior commissure - posterior commissure line (positive = superior).

R/L = right/left

BA = Brodman area

VAN = Ventral anterior nucleus

VLN = Ventral lateral nucleus

Table 2: Voxel with positive peak loadings on the canonical image, left posterior cingulate-hippocampus connectivity

Region	Side	Coordinates (mm)		
		x	y	z
Precuneus	R	18	-55	38
	R	10	-47	36
Insula	L	-43	12	4
Inferior Temporal Gyrus	R	49	-3	-36
	R	61	-39	-17
	L	-45	13	-35
Middle Temporal Gyrus	L	-42	-64	23
	L	-63	-56	4
Lingual Gyrus	R	15	-72	5
Middle Occipital Gyrus	L	-57	-64	-7
Fusiform gyrus	L	-61	-48	-21
Parahippocampal Gyrus	L	-30	-34	-9
	L	-21	-38	4
Hippcoampus	R	8	-52	3
	R	49	-19	-14
Precentral Gyrus	L	-46	-10	32
Cerebellum (Uvula, Culmen, Declive, Pyramis)	R	26	-84	-25
	R	32	-45	-26
	L	-10	-62	-15
	L	-11	-69	-27
	L	-24	-86	-24
	L	-1	-53	0

Region	Side	Coordinates (mm)		
		x	y	z
Cerebellum (Uvula, Culmen, Declive, Pyramis)	L	-38	-37	-28

Voxel with positive loading above the 98th percentile. Brain regions are indicated by Talairach and Tournoux coordinates, x, y and z(Talairach and Tournoux, 1988): x = the medial to lateral distance relative to midline (positive = right hemisphere); y = the anterior to posterior distance relative to the anterior commissure (positive = anterior); z = superior to inferior distance relative to the anterior commissure -posterior commissure line (positive = superior).

R/L = right/left

Table 3: Voxel with positive peak loadings on the canonical image, right posterior cingulate-hippocampus connectivity

		Coordinates (mm)		
Region	**Side**	**x**	**y**	**z**
Precuneus	R	18.0	-55.0	39.0
	R	9.0	-46.0	37.0
Posterior Cingulate	R	6.0	-55.0	6.0
	R	19.0	-59.0	7.0
Cingulate Gyrus	L	-8.0	-45.0	36.0
Superior Parietal Lobule	L	-34.0	-54.0	50.0
Insula	L	-43.0	11.0	4.0
Inferior Temporal Gyrus	R	50.0	-4.0	-37.0
	R	61.0	-39.0	-17.0
	L	-46.0	11.0	-35.0
	L	-50.0	-5.0	-38.0
Middle Temporal Gyrus	R	51.0	-70.0	16.0
	L	-41.0	-63.0	23.0
	L	-63.0	-56.0	4.0
	L	-53.0	-58.0	9.0
Lingual Gyrus	R	15.0	-72.0	5.0
	R	12.0	-85.0	1.0
	L	-12.0	-54.0	5.0
Middle Occipital Gyrus	L	-46.0	-74.0	5.0
Fusiform gyrus	L	-62.0	-46.0	-20.0
Parahippocampal Gyrus	L	-21.0	-38.0	4.0
Hippcoampus	R	47.0	-19.0	-15.0

		Coordinates (mm)		
Region	**Side**	**x**	**y**	**z**
Hippocampus	L	-33.0	-30.0	-9.0
Uncus	R	14.0	-1.0	-29.0
Cerebellum (Culmen, Declive)	R	32.0	-45.0	-26.0
	R	24.0	-86.0	-21.0
	L	-2.0	-53.0	1.0
	L	-38.0	-36.0	-29.0

Voxel with positive loading above the 98th percentile. Brain regions are indicated by Talairach and Tournoux coordinates, x, y and z(Talairach and Tournoux, 1988): x = the medial to lateral distance relative to midline (positive = right hemisphere); y = the anterior to posterior distance relative to the anterior commissure (positive = anterior); z = superior to inferior distance relative to the anterior commissure -posterior commissure line (positive = superior).

R/L = right/left

Figure 1: Default mode network (mixed-effects second level analysis)

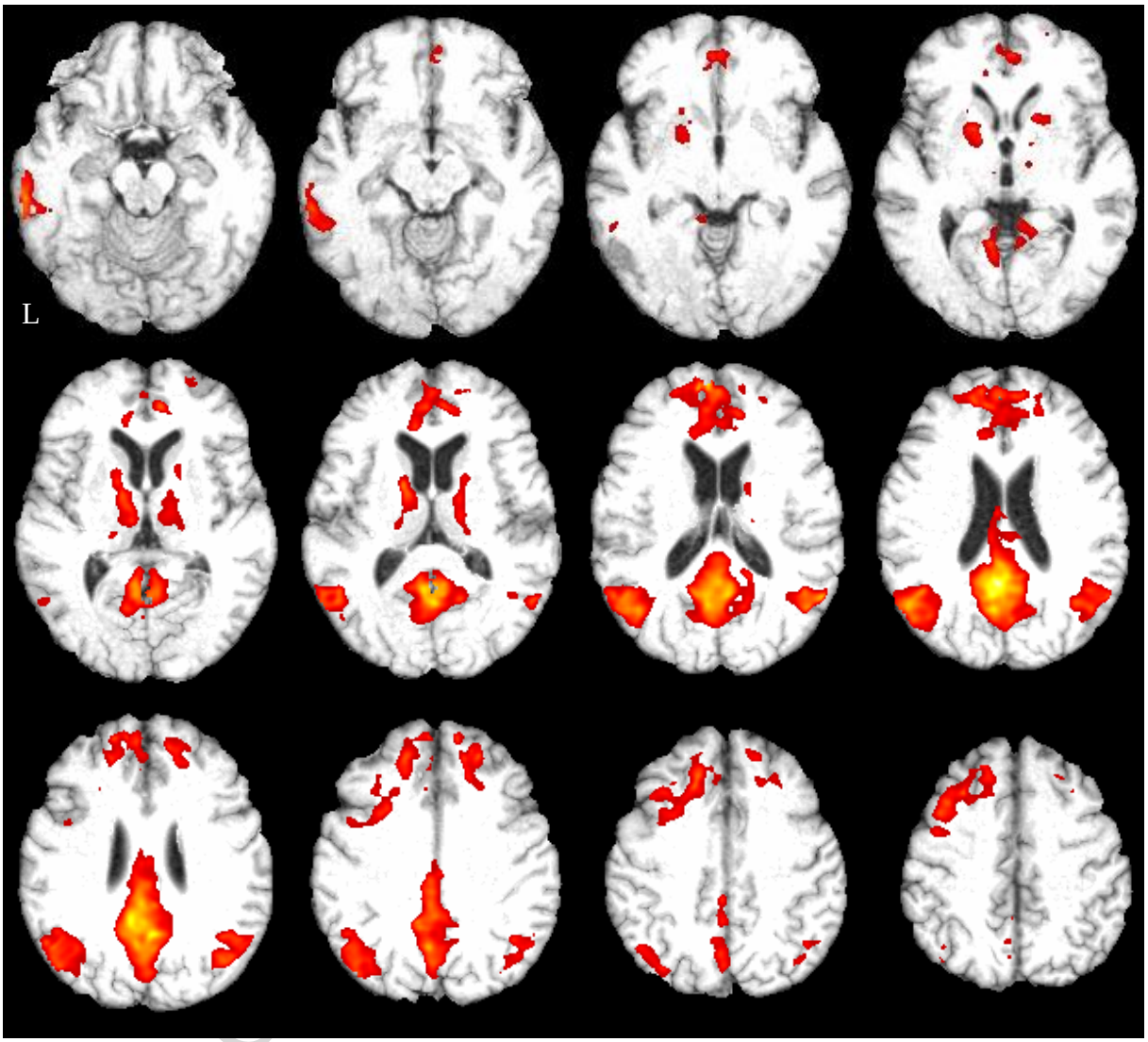

Figure 2: Default mode network (ICA analysis)
Figure 2a: Axial slices

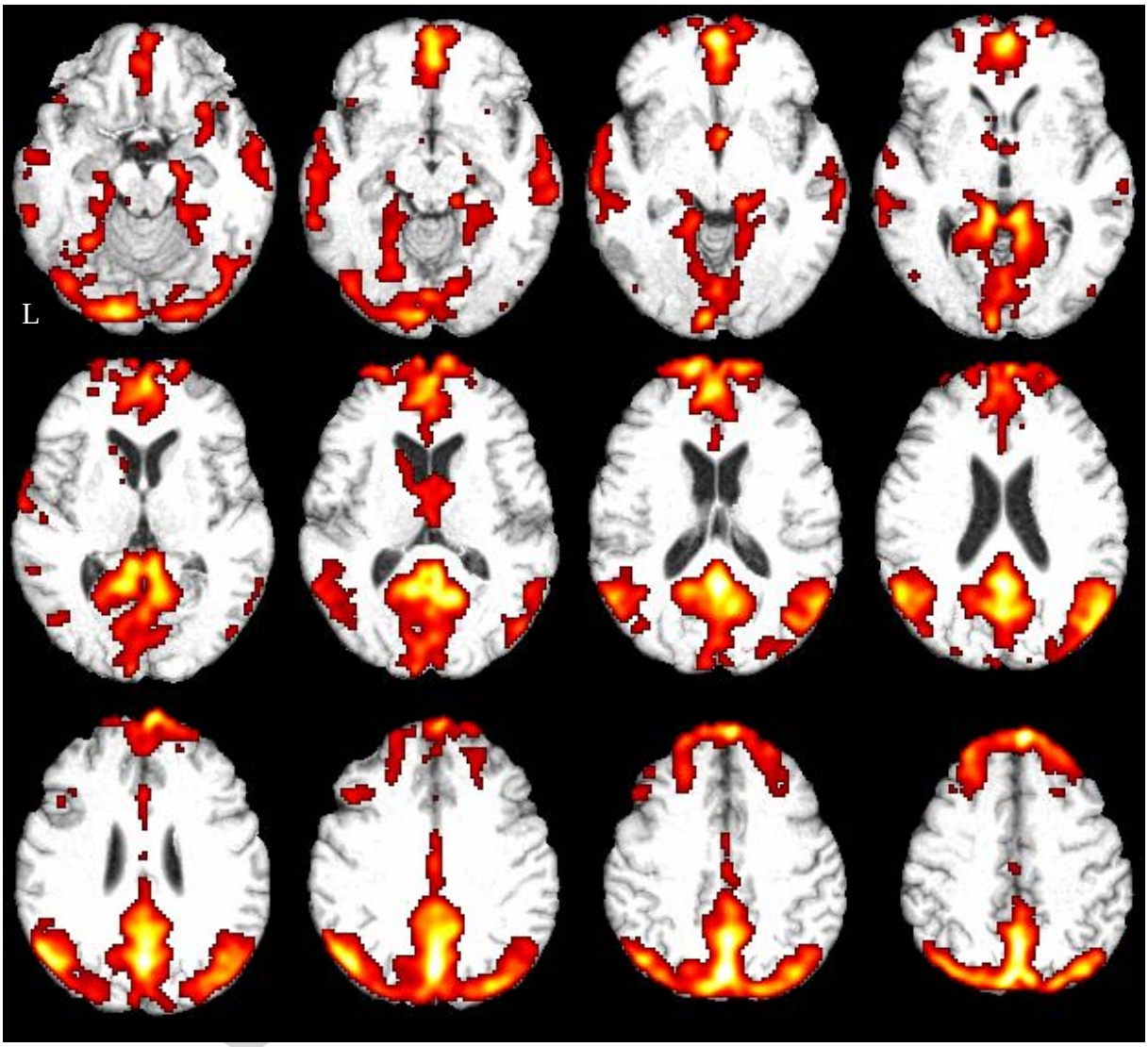

Figure 2b: coronal slices

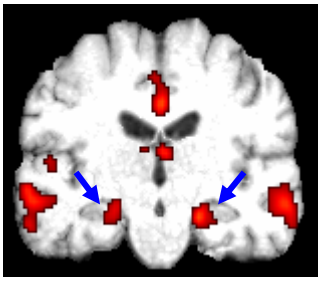

Figure 3: Functional connectivity between posterior cingulate and hippocampus and FA
Figure 3a: Axial sections

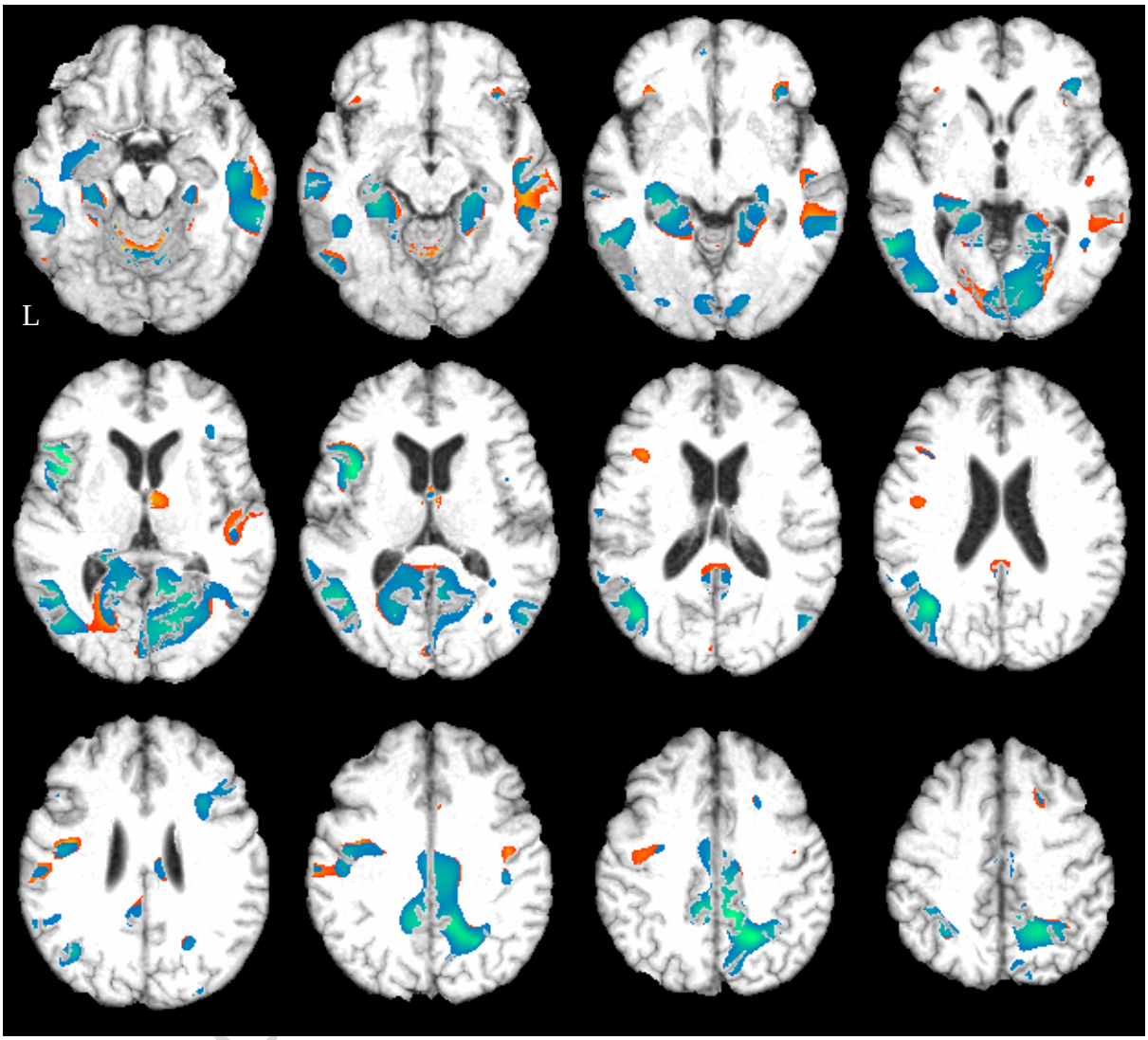

Figure 3b: Paramidsagittal sections

Right

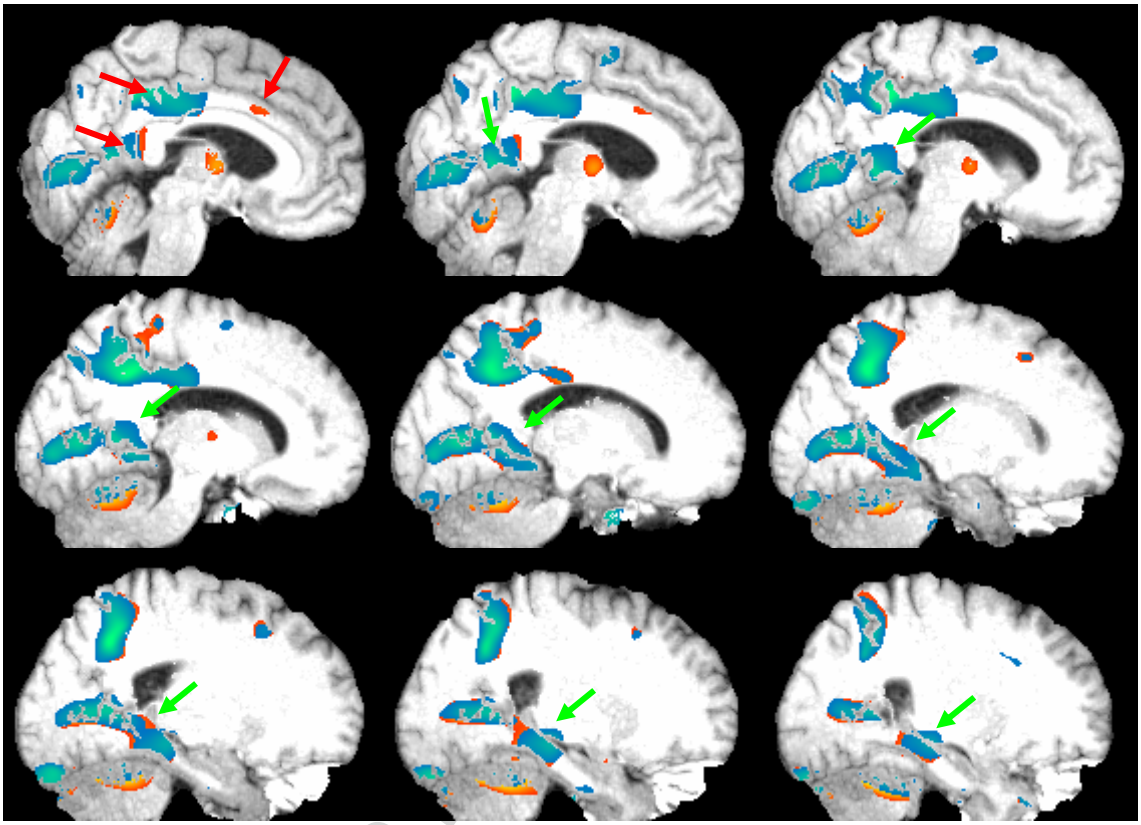

Left

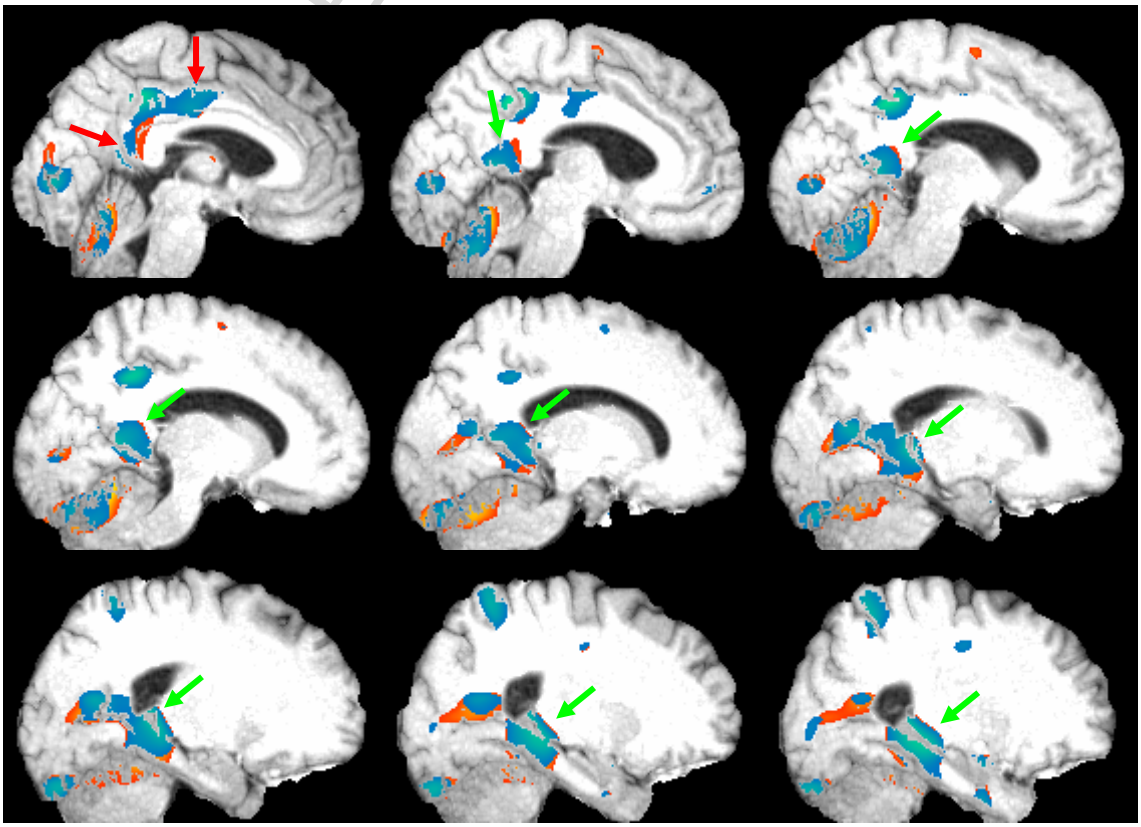

Figure 4: Functional connectivity between left posterior cingulate and hippocampus connectivity and MD

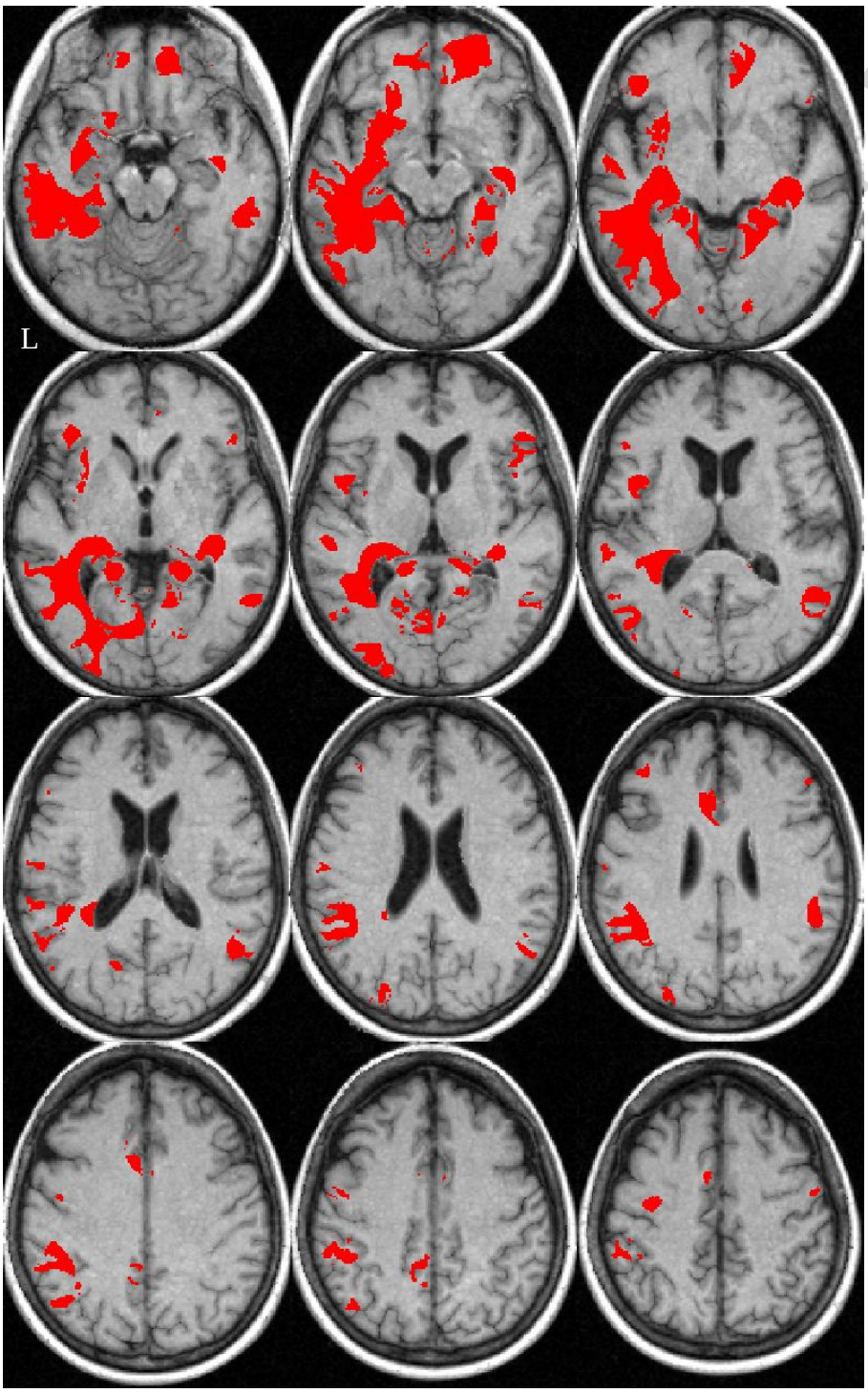

The negative component of the first canonical image with left posterior cingulate-hippocampus connectivity regressed on MD, representing lower MD values with higher connectivity. The effects are projected on the rendered axial sections of the T1-weighted template brain. Sections go from ventral at Talairach-Tournoux coordinate z = -16 to

dorsal at z = 48, sections are 6 mm apart. Right of image is right of brain (view from superior).

Figure 5:

Figure 5a: fMRI

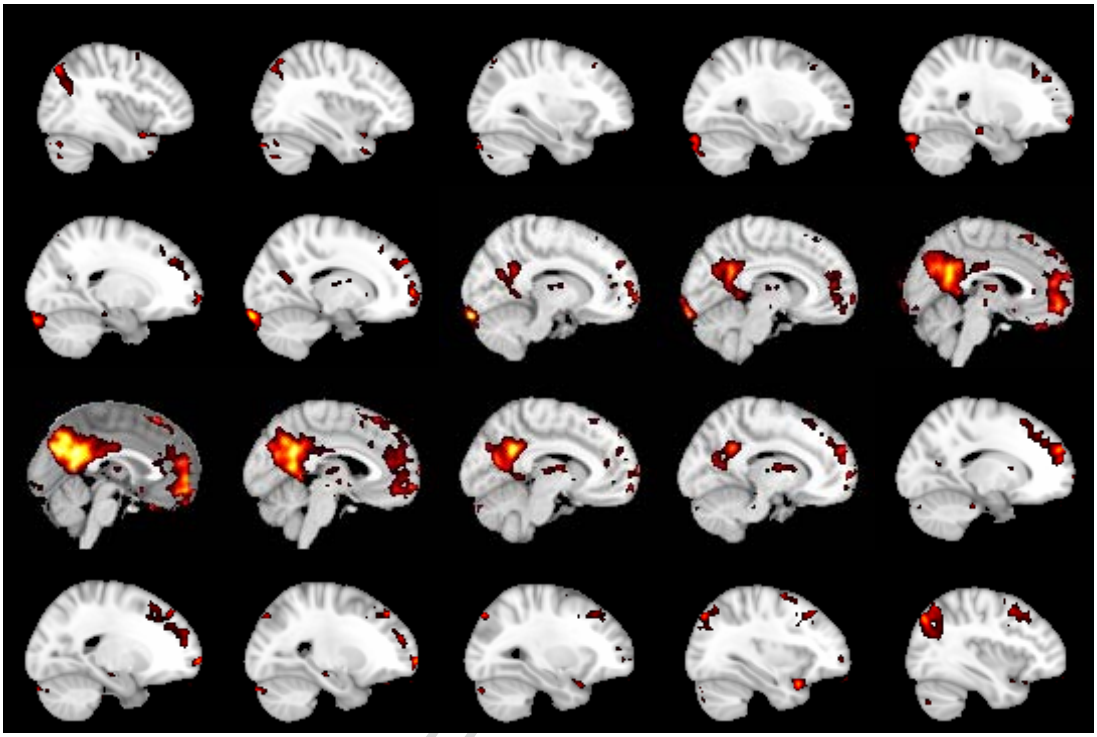

Figure 5b: DTI